

Asymptotic Description of Schematic Models for CKN

Matthias Sperl

Duke University, Department of Physics, Box 90305, Durham, NC 27708, USA

Abstract

The fits of $0.4Ca(NO_3)_2 \cdot 0.6K(NO_3)$ (CKN) by schematic mode-coupling models [V. Krakoviack and C. Alba-Simionesco, *J. Chem. Phys.* **117**, 2161-2171 (2002)] are analyzed by asymptotic expansions. The validity of both the power-law and the Cole-Cole-peak solutions for the critical spectrum are investigated. It is found that the critical spectrum derived from the fits is described by both expansions equally well when both expansions are carried out up to next-to-leading order. The expansions up to this order describe the data for 373K over two orders of magnitude in frequency. In this regime an effective power law ω^a can be identified where the observed exponent a is smaller than its calculated value by about 15%; this finding can be explained by corrections to the leading-order terms in the asymptotic expansions. For higher temperatures, even smaller effective exponents are caused by a crossover to the alpha-peak spectrum.

Key words: dynamic light scattering, glass transition, molten salts, mode coupling

PACS: 64.70.Pf, 33.55.Fi, 61.20.Lc, 61.25.Em

1 Introduction

For a given interaction potential mode-coupling theory (MCT) in its microscopic version can predict the transition from a fluid to a glass [1]. Close to the transition, the glassy dynamics is ruled by universal scaling laws, that are independent of the details of the interactions. These universal laws have been applied frequently to describe experimental data, especially when the microscopic details are difficult to model, which is the case in most molecular glass formers. At larger distances from the liquid-glass transition, non-universal corrections to scaling

become important [2]. These can be calculated exactly by asymptotic expansion for a given MCT model, but introduce additional parameters for the fitting of data. An alternative to fitting higher-order terms of an asymptotic expansion is provided by schematic MCT models. These simplified models incorporate naturally both universal features and corrections, and can be used to fit data by a limited number of parameters. Similar to the microscopic models, asymptotic expansions can also be devised for the schematic models for experimentally relevant parameters, which in turn provides insight into the validity of the universal laws

and the importance of the corrections for the data under investigation.

One particular schematic model used frequently is the F_{12} model which deals with a single correlator mimicking the density-correlators [3]. This model can be supplemented by a second correlator to describe some specific probe variable [4]; and this two-correlator model has been applied successfully to the description of experimental data [5,6,7,8,9,10]. Data for salol [11] and benzophenone (BZP) [12] were fitted recently by this model, and it was subsequently shown that an apparent violation of universal MCT formulas [13,12] can be reconciled with a more detailed asymptotic analysis within MCT [14,15]: A Cole-Cole peak found earlier for this schematic model [16,17] was identified in the fits for these two substances. While the asymptotic approximation by the Cole-Cole peak improved the description of salol only quantitatively, the presence of a Cole-Cole peak was essential for interpreting the BZP spectra even qualitatively. A remarkable wing in the Giga-Hertz regime could be explained by a significant contribution of the Cole-Cole peak [15,18].

Another substance studied in detail is the molten salt $0.4Ca(NO_3)_2 \cdot 0.6K(NO_3)$ (CKN) which was measured in light-scattering experiments [19]. These data were successfully fitted by a number of different schematic models [20,21]. For these models the asymptotic expansions will be derived in an effort to identify asymptotic features present in the data of CKN. The models will be introduced in Sec. 2, their asymptotic solutions presented in Sec. 3; Sec. 4

discusses the two lowest temperatures considered in [21], Sec. 5 extends the analysis down to temperatures as low as in Ref. [20], and presents a conclusion.

2 Schematic Model Fits

MCT provides equations of motion for correlation functions $\phi_q(t)$ where the index q denotes the wave-number or a specific dynamical variable. With the initial conditions $\phi_q(t=0) = 1$ and $\partial_t \phi_q(t=0) = 0$, the MCT equations read

$$\begin{aligned} & \partial_t^2 \phi_q(t) + v_q \partial_t \phi_q(t) + \Omega_q^2 \phi_q(t) \\ & + \Omega_q^2 \int_0^t dt' m_q(t-t') \partial_{t'} \phi_q(t') = 0, \end{aligned} \quad (1)$$

where Ω_q and v_q specify normal liquid dynamics. In the F_{12} model, the dynamics of the density correlators is modeled by a single correlation function with kernel

$$m(t) = v_1 \phi(t) + v_2 \phi(t)^2. \quad (2)$$

The probing variable is given by a second correlator $\phi_A(t)$ and a corresponding kernel [4],

$$m_A(t) = v_A \phi(t) \phi_A(t). \quad (3)$$

The dynamics of $\phi_q(t)$ is given by Eq. (1) with q replaced by A . A different kernel for a second correlator was introduced by Alba-Simionesco and coworkers that shall be denoted by $\phi_r(t)$ [22],

$$m_r(t) = r m(t) = r [v_1 \phi(t) + v_2 \phi(t)^2]. \quad (4)$$

In addition, a number of effective correlators $\phi_s(t)$ were defined, some of whose were originally motivated to capture the DID mechanism [22,21],

$$\phi_s(t) = \gamma\phi(t)^2 + (1 - \gamma)\phi_{A,r}(t)^2, \quad (5a)$$

$$\phi_s(t) = \gamma\phi(t)^2 + (1 - \gamma)\phi_{A,r}(t), \quad (5b)$$

$$\phi_s(t) = \gamma\phi(t) + (1 - \gamma)\phi_{A,r}(t)^2, \quad (5c)$$

$$\phi_s(t) = \gamma\phi(t) + (1 - \gamma)\phi_{A,r}(t). \quad (5d)$$

Here, $\phi_{A,r}(t)$ denotes a second correlator with the kernel from Eq. (3) or Eq. (4), respectively. The data was fitted with the susceptibility given by the Fourier transformation

$$\chi_s''(\omega) = \omega \int_0^\infty dt \cos(\omega t) \phi_s(t). \quad (6)$$

Further details and the values of the fit parameters can be found in Refs. [21,23]. The fit curves are reproduced in Fig. 1 together with the experimental data for CKN for the two lowest temperatures considered in [21]. Here, kernel (4) and the effective correlator (5a) are applied; the frequencies are denoted in units of $\nu = \omega/(2\pi)$.

3 Asymptotic Solution for Schematic Models

The general asymptotic formulas for the critical spectrum are given in the following and are specialized to the schematic models subsequently. From those formulas the asymptotic description of CKN shall be inferred. The following discussion is restricted to spectra directly at the transition point, which will be called critical spectra.

Such a critical spectrum is shared by larger and larger parts of the dynamics when the temperature is approaching the critical temperature T_c . Two different asymptotic approximations for the critical spectrum shall be used, a well-known power-law expansion and a modified Cole-Cole law introduced recently.

The power-law solution for the critical spectrum is derived from the asymptotic expansion for the correlators. It reads up to next-to-leading order [2],

$$\chi_q''(\omega) = [\Gamma(1 - a) \sin(\pi a/2)] h_q(\omega t_0)^a \times [1 + k_a \hat{K}_q(\omega t_0)^a], \quad (7a)$$

with the prefactor

$$k_a = 2\Gamma(1 - a) \cos(\pi a/2) / \lambda, \quad (7b)$$

the critical amplitude h_q , the critical exponent a – given by the exponent parameter λ using the Euler- γ function in $\lambda = \Gamma(1 - a)^2 / \Gamma(1 - 2a)$ – the microscopic time scale t_0 , and a correction amplitude \hat{K}_q . The first line in Eq. (7a) constitutes the leading-order result: an increase of the critical spectrum with as ω^a .

In contrast to Eq. (7), the modified Cole-Cole law is obtained from using the expansion for the kernel $m_q(t)$ rather than the one for $\phi_q(t)$ [15]:

$$\chi_q(\omega) = \chi_{0q}^{cc} / [1 + (-i\omega/\omega_q^c)^a + \hat{K}_q^{cc} (-i\omega/\omega_q^c)^{2a}], \quad (8a)$$

where all parameters can be cast in a form using only results known from the power-law expansion. The amplitude is

given by

$$\chi_{0q}^{cc} = 1 - f_q^c, \quad (8b)$$

with the glass-form factor f_q^c ; the characteristic frequency reads

$$\omega_q^c t_0 = [(1 - f_q^c) / (h_q \Gamma(1 - a))]^{1/a}, \quad (8c)$$

and the correction amplitude is expressed as

$$\hat{K}_q^{cc} = 1 + [(1 - f_q^c) / h_q] \hat{K}_q / \lambda. \quad (8d)$$

For $\hat{K}_q^{cc} = 0$, the correction vanishes, and the leading-order result in Eq. (8a) is recovered as the original Cole-Cole function [27].

For the schematic models used in the following, one can rewrite all the parameters needed in Eqs. (7) and (8) in terms of only two variables: the exponent parameter λ and the respective coupling parameters, v_A or r . We obtain for the glass-form factors,

$$\begin{aligned} f^c = 1 - \lambda, \quad f_A = \frac{v_A(1 - \lambda) - 1}{v_A(1 - \lambda)}, \\ f_r = \frac{r(1 - \lambda)}{r(1 - \lambda) + \lambda}, \end{aligned} \quad (9a)$$

for the critical amplitudes,

$$\begin{aligned} h = \lambda, \quad h_A = \lambda / [v_A(1 - \lambda)^2], \\ h_r = \frac{r\lambda}{[r(1 - \lambda) + \lambda]^2}, \end{aligned} \quad (9b)$$

and for the correction amplitudes,

$$\begin{aligned} \hat{K} = \kappa, \\ \hat{K}_A = \kappa + \frac{\lambda}{1 - \lambda} \left[\frac{v_A(1 - \lambda)}{v_A - 1/(1 - \lambda)} - 1 \right], \\ \hat{K}_r = \kappa + \lambda^2 \frac{1 - r}{r(1 - \lambda) + \lambda}. \end{aligned} \quad (9c)$$

κ can be determined straightforwardly from the exponent parameter λ [17]. For the discussion below, κ will always contribute only a very small part to the correction amplitude; assuming $\kappa = 0$ would not alter any results significantly.

The models for the second correlators in Eqs. (3) and (4) are in fact very similar, and the preceding formulas also motivate a closer comparison. From setting $f_A = f_r$, one obtains a mapping between the coupling coefficients,

$$r = v_A \lambda - \frac{\lambda}{1 - \lambda}, \quad v_A = \frac{r}{\lambda} + \frac{1}{1 - \lambda}. \quad (10)$$

When v_A and r are related by Eq. (10), the ratio between the critical amplitudes becomes

$$\frac{h_A}{h_r} = \lambda + \frac{\lambda^2}{r(1 - \lambda)}, \quad (11)$$

which becomes unity for $r = \lambda^2 / (1 - \lambda)^2$. For that specific value of r , the mapping (10) is correct in leading asymptotic order: $\chi_A''(\omega)$ and $\chi_r''(\omega)$ have the same leading-order approximation in both Eq. (7a) and (8a). Imposing again Eq. (10), the ratio among the correction amplitudes is

$$\frac{\hat{K}_A - \kappa}{\hat{K}_r - \kappa} = 1 + \frac{\lambda}{r(1 - \lambda)}, \quad (12)$$

which cannot be unity with h_a/h_r simultaneously. However, the correction amplitudes get closer to each other for larger values of r . Typical values for r and v_A can be obtained from Ref. [21]; there, both models for the second correlator were used for fitting the CKN data independently. The values reported in Ref. [21] agree within

a 15% margin with the mapping in Eq. (10); the values for r also allow for an approximate identification of the amplitudes, $h_A \approx h_r$, and the ratio in Eq. (12) lies between a maximum of 2 and a minimum as low as 1.2. Two conclusions can be drawn from the preceding discussion. First, both models, $\chi''_A(\omega)$ and $\chi''_r(\omega)$, are almost equivalent in their asymptotic properties for experimentally relevant parameter values; and second, the fitting procedures employed in Ref. [21] show this equivalence consistently.

The asymptotic expansions for the effective correlators and their spectra are calculated by inserting the results for $\phi(t)$ and $\phi_{A,r}$ into Eq. (5) and retaining only terms up to second order. For the case (5a) one gets,

$$\begin{aligned} f_s &= \gamma f^{c2} + (1 - \gamma) f_{A,r}^2, \\ h_s &= 2\gamma f^c h + 2(1 - \gamma) f_{A,r} h_{A,r}, \\ \hat{K}_s &= [\gamma(h^2 + 2f^c h \hat{K}) + (1 - \gamma) \\ &\quad \times (h_{A,r}^2 + 2f_{A,r} h_{A,r} \hat{K}_{A,r})] / h_s. \end{aligned} \quad (13)$$

The remaining cases from Eq. (5) can be calculated in the same way and yield similar formulas, so these results need not be given here. The parameters for the Cole-Cole law result from inserting the values from Eq. (13) into Eq. (8) with $q = s$.

4 Results

The results shown in this section will be restricted to temperatures at and above 383K as in [21]. There, this restriction was motivated to avoid the artefacts in the original data [19] identified for lower temperatures [24,25,26].

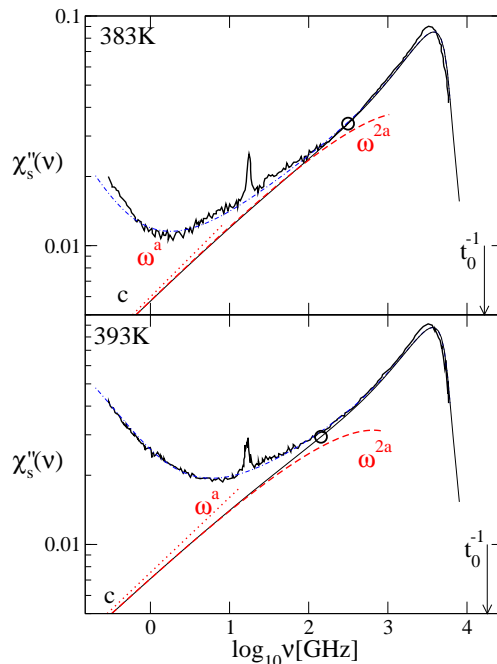


Fig. 1. Power-law expansion for CKN. The full curves reproduce the data from Ref. [19]. The dashed-dotted curves present schematic-model fits using kernel (4) and the effective correlator (5a) with $r = 8.6$ as in [21]. The full lines labeled c display the critical spectra for $\lambda = 0.656$ ($a = 0.344$, upper panel) and $\lambda = 0.7$ ($a = 0.327$, lower panel), respectively. The dotted lines labeled ω^a and the dashed lines labeled ω^{2a} show the leading and next-to-leading order result of Eq. (7a). The points where the critical spectra deviate by 10% from the approximation by (7a) are indicated by circles.

However, the results derived for the critical spectrum in the present section will be shown to be relevant also for lower temperatures in Sec. 5. For the discussion of the critical spectrum, an appropriate point on the transition surface of the F_{12} model needs to be fixed. In the F_{12} model such a critical point can be specified uniquely by the value of λ . One reasonable choice is a transition point close to the fit parameters for the lowest temperature under discussion.

Such a point is chosen for the critical spectrum shown in the upper panel of Fig. 1; the exponent parameter for this critical point is $\lambda = 0.656$. Another way to determine a suitable transition point is suggested by an extrapolation procedure in Ref. [21], where $\lambda \approx 0.7$ is proposed for the description of the dynamics. The critical spectrum for the transition point satisfying $\lambda = 0.7$ is added to the lower panel of Fig. 1; to show also experimental results close to that transition point, data and fit of the nearby 393K spectrum is added.

The asymptotic approximation by Eq. (7a) is shown in Fig. 1, and it is seen clearly that the leading-order power law describes the critical spectrum only for $\nu \lesssim 1\text{GHz}$, regardless of the chosen transition point. Including the correction describes the critical solutions up to 300GHz and 150GHz, respectively. However, Eq. (7a) explains the measured spectrum for 383K for only about one order of magnitude in frequency. The apparent power-law behavior $\nu^{a'}$ with $a' = 0.22$ between 2GHz and 200GHz for 383K does in turn not show the asymptotic value $a = 0.344$ for the critical exponent. This is because the separation of this state point from the transition is too large.

The alternative asymptotic approximation by the Cole-Cole law, Eq. (8a), is shown in Figure 2. Similar to the power-law solution, the leading-order Cole-Cole formula applies to the critical spectra only for $\nu < 1\text{GHz}$, but has no relevance for the description of the present data. The formula including the correction describes the critical spectra in upper and lower panel for

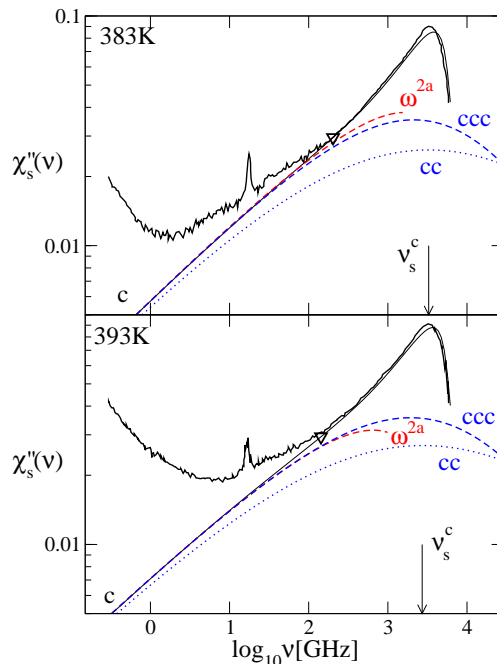


Fig. 2. Cole-Cole law for CKN. The full curves display the experimental data [19] as before. Also reproduced from Fig. 1 are the respective critical spectra (c) and the power-law approximations by Eq. (7) up to next-to-leading order (ω^{2a}). The dotted line labeled cc and the dashed line labeled ccc show the leading- and next-to-leading order approximation by the Cole-Cole law, Eq. (8a) for frequencies indicated by the arrows. A 10% deviation of the critical spectra from their respective approximation by Eq. (8a) are shown by the triangles.

$\nu < 200\text{GHz}$ and $\nu < 150\text{GHz}$, respectively. The comparison of both panels also reveals that the choice of a particular transition point does not lead to major differences. In both cases, Cole-Cole and power-law expansion are practicably indistinguishable for $\nu \lesssim 500\text{GHz}$. This is also the regime where they both approximate the critical spectrum well.

As seen in Fig. 1, the range of validity for approximation (7a) increases by two decades when the corrections

	I	II	III	IV	V	VI
ϕ_s	(4), (5a)	(4), (5b)	(4), (5c)	(4), (5d)	(3), (5a)	(3), (5d)
λ	0.656	0.644	0.642	0.629	0.630	0.644
\hat{K}_s	-0.31	-0.24	-0.32	-0.28	-0.26	-0.32
v_s^c [GHz]	3280	3060	2650	2980	2750	2410
χ_{0s}^{cc}	0.496	0.491	0.483	0.478	0.510	0.507
\hat{K}_s^{cc}	0.63	0.68	0.67	0.68	0.67	0.59

Table 1

Selected parameter values for the asymptotic approximation of the critical spectra. The designation of the cases I–VI is the same as in [21]; the first line shows the definition of the effective correlator ϕ_s .

are included, $\hat{K}_s = -0.31$ for the upper panel; such a value for \hat{K}_s can be considered moderate compared to BZP and salol where the corresponding values are around five times larger [15]. For the lower panel $\hat{K}_s = -0.44$. On the contrary in Fig. 2, the corrections in (8d) for approximation (8a) are much larger for CKN, $\hat{K}_s^{cc} = 0.63$ and $\hat{K}_s^{cc} = 0.54$ for upper and lower panel, than for BZP and salol where the corrections are always close to zero for the Cole-Cole law. Table 1 lists the values of characteristic parameters for the models used in Ref. [21]. Model I is the one discussed in detail above for Figs. 1 and 2. Most parameters are remarkably similar throughout all the models. The location of the Cole-Cole peak v_s^c varies by only 30%, so the scenario shown in Fig. 2 is typical for all these models. The values for the case $\lambda = 0.7$, corresponding to the lower panels in Figs. 1 and 2, are very similar and are therefore omitted.

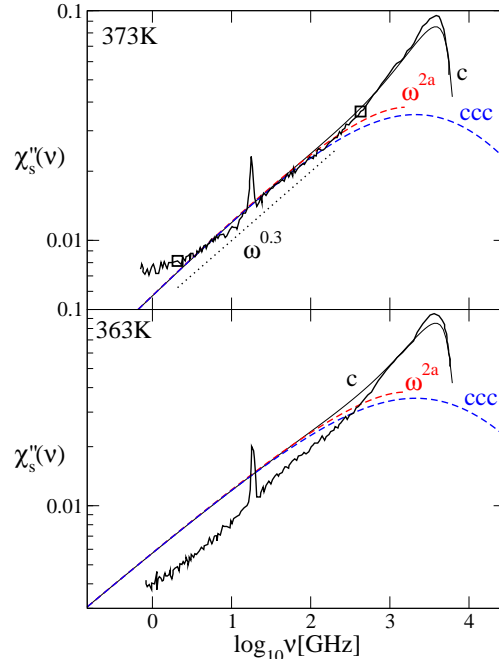


Fig. 3. Spectra for 373K and 363K. Critical spectrum (c), power-law approximation (ω^{2a}) and Cole-Cole law (ccc) are reproduced from Figs. 1 and 2. In the upper panel, the squares indicate a 10% deviation of the approximation (7) from the data. An effective power law $\omega^{0.3}$ is shown as dotted line.

5 Discussion

Figures 1 and 2 indicate that both the approximations, Eq. (7a) and (8a), as

well as the full critical spectra do not describe significant parts of the measured data for $T \geq 383\text{K}$. For lower temperatures, two additional spectra with fits from Ref. [20] are available, $T = 373\text{K}$ and $T = 363\text{K}$. The data for these temperatures from Ref. [19] are shown in Fig. 3. It is apparent from the upper panel of Fig. 3 that the spectrum for $T = 373\text{K}$ coincides with the critical spectrum for 2.5 decades; the asymptotic expansions describe the data for over two orders of magnitude.

The corrections to the power law, cf. Eq. (7a), lead to a renormalization of the asymptotic power law $\omega^{0.344}$ to an effective power law $\omega^{0.3}$. In contrast to the findings for salol and BZP, the Cole-Cole formula (8a) is not essential for understanding these smaller exponents for CKN [14,15]. The asymptotic expansions also reveal that the minimum seen in the data for CKN can be regarded as a β -minimum with a von Schweidler wing for lower and a critical spectrum for higher frequencies. Therefore, for temperatures $T \gtrsim 383\text{K}$, earlier analyses of the minimum can be justified [28].

For the 373K spectrum a fit can be found with the same parameters as for $T = 383\text{K}$ by adjusting ν_1 and ν_2 only. The resulting state is in fact close to the critical point for $\lambda = 0.656$, and a similar point was found earlier for the same temperature for slightly different parameters [20]. The situation for $T = 363\text{K}$ is different. The spectrum shown in the lower panel of Fig. 3 deviates drastically from the critical spectrum for $\nu < 1\text{THz}$. Hence, in this case also the approximations to the critical spectrum are not applicable. Although

the data for $T = 363\text{K}$ could be fitted in [20], this was possible only by moving away from the path for higher temperatures rather considerably [21]. One might interpret that as an indication of the mentioned experimental artefacts [21,24,25,26].

For temperatures $T \leq 363\text{K}$, the exponents reported in Fig. 4 of Ref. [25] are all equal or larger than 0.4. These temperatures, when interpreted within MCT, are therefore located below T_c . This is a consequence of the evolution of the spectra as seen for higher temperatures, as well as the asymptotic analysis at the critical point: Both mechanisms only allow for *smaller* effective exponents compared to the asymptotic value for a which cannot be larger than 0.396. Below T_c , larger effective exponents are not in contradiction to MCT; however, they do not describe a critical spectrum.

In conclusion, for $T \leq 363\text{K}$, in the spectra from [19] as well as [25] no critical MCT spectrum can be demonstrated; $T = 383\text{K}$ marks the highest temperature where part of the critical spectrum is observable; and the data for 373K, cf. upper panel of Fig. 3, exhibit the critical MCT spectrum rather convincingly.

ACKNOWLEDGEMENTS I want to thank V. Krakoviack for providing the fit parameters from Refs. [21,23]. Discussions with W. Götze and V. Krakoviack are gratefully appreciated. This work was supported by DFG Grant No. SP 714/3-1 and SP 714/5-1, and NSF grants DMR0137119 and DMS0244492.

References

- [1] U. Bengtzelius, W. Götze, A. Sjölander, *J. Phys. C* 17 (1984) 5915.
- [2] T. Franosch, M. Fuchs, W. Götze, M. R. Mayr, A. P. Singh, *Phys. Rev. E* 55 (1997) 7153.
- [3] W. Götze, *Z. Phys. B* 56 (1984) 139.
- [4] L. Sjögren, *Phys. Rev. A* 33 (1986) 1254.
- [5] A. P. Singh, G. Li, W. Götze, M. Fuchs, T. Franosch, H. Z. Cummins, *J. Non-Cryst. Solids* 235–237 (1998) 66.
- [6] B. Rufflé, C. Ecolivet, B. Toudic, *Europhys. Lett.* 45 (1999) 591.
- [7] W. Götze, T. Voigtmann, *Phys. Rev. E* 61 (2000) 4133.
- [8] A. Brodin, M. Frank, S. Wiebel, G. Shen, J. Wuttke, H. Z. Cummins, *Phys. Rev. E* 65 (2002) 051503.
- [9] S. Wiebel, J. Wuttke, *New J. Phys.* 4 (2002) 56.
- [10] H. Cang, J. Li, H. C. Andersen, M. D. Fayer, *J. Chem. Phys.* 123 (2005) 064508.
- [11] G. Hinze, D. D. Brace, S. D. Gottke, M. D. Fayer, *Phys. Rev. Lett.* 84 (2000) 2437.
- [12] H. Cang, V. N. Novikov, M. D. Fayer, *Phys. Rev. Lett.* 90 (2003) 197401.
- [13] M. Ricci, P. Bartolini, R. Torre, *Philos. Mag. B* 82 (2002) 541.
- [14] W. Götze, M. Sperl, *Phys. Rev. Lett.* 92 (2004) 105701.
- [15] W. Götze, M. Sperl, to be published.
- [16] G. Buchalla, U. Dersch, W. Götze, L. Sjögren, *J. Phys. C* 21 (1988) 4239.
- [17] W. Götze, L. Sjögren, *J. Phys.: Condens. Matter* 1 (1989) 4183.
- [18] H. Z. Cummins, *J. Phys.: Condens. Matter* 17 (2005) 1457.
- [19] G. Li, W. M. Du, X. K. Chen, H. Z. Cummins, N. J. Tao, *Phys. Rev. A* 45 (1992) 3867.
- [20] V. Krakoviack, C. Alba-Simionesco, M. Krauzman, *J. Chem. Phys.* 107 (1997) 3417.
- [21] V. Krakoviack, C. Alba-Simionesco, *J. Chem. Phys.* 117 (2002) 2161.
- [22] C. Alba-Simionesco, M. Krauzman, *J. Chem. Phys.* 102 (1995) 6574.
- [23] V. Krakoviack, Ph.D. thesis, Université Paris XI Orsay (2000).
- [24] N. V. Surovtsev, J. A. H. Wiedersich, N. V. Novikov, E. Rössler, A. P. Sokolov, *Phys. Rev. B* 58 (1998) 14888.
- [25] J. Gapinski, W. Steffen, A. Patkowski, A. P. Sokolov, K. Kisliuk, U. Buchenau, M. Russina, F. Mezei, H. Schober, *J. Chem. Phys.* 110 (1999) 2312.
- [26] H. C. Barshilia, G. Li, G. Q. Shen, H. Z. Cummins, *Phys. Rev. E* 59 (1999) 5625.
- [27] K. S. Cole, R. H. Cole, *J. Chem. Phys.* 9 (1941) 341.
- [28] H. Z. Cummins, W. M. Du, M. Fuchs, W. Götze, S. Hildebrand, A. Latz, G. Li, N. J. Tao, *Phys. Rev. E* 47 (1993) 4223.